

Disc precession in the M31 dipping X-ray binary Bo 158?

R. Barnard,^{1*} S. B. Foulkes,¹ C. A. Haswell,¹ U. Kolb,¹
 J. P. Osborne² and J. R. Murray³

¹*The Open University, Walton Hall, Milton Keynes, Buckinghamshire, MK7 6AA, UK*

²*The University of Leicester, University Road, Leicester, LE1 7RH, UK*

³*Swinburne University of Technology, PO Box 218, Hawthorne, Victoria 3122, Australia*

Accepted 2005 November 7. Received 2005 February 16

ABSTRACT

We present results from three XMM-Newton observations of the M31 low mass X-ray binary XMMU J004314.4+410726.3 (Bo 158), spaced over 3 days in 2004, July. Bo 158 was the first dipping LMXB to be discovered in M31. Periodic intensity dips were previously seen to occur on a 2.78-hr period, due to absorption in material that is raised out of the plane of the accretion disc. The report of these observations stated that the dip depth was anti-correlated with source intensity. In light of the 2004 XMM-Newton observations of Bo 158, we suggest that the dip variation is due to precession of the accretion disc. This is to be expected in LMXBs with a mass ratio $\lesssim 0.3$ (period $\lesssim 4$ hr), as the disc reaches the 3:1 resonance with the binary companion, causing elongation and precession of the disc. A smoothed particle hydrodynamics simulation of the disc in this system shows retrograde rotation of a disc warp on a period of $\sim 11 P_{\text{orb}}$, and prograde disc precession on a period of $29 \pm 1 P_{\text{orb}}$. This is consistent with the observed variation in the depth of the dips. We find that the dipping behaviour is most likely to be modified by the disc precession, hence we predict that the dipping behaviour repeats on a 81 ± 3 hr cycle.

Key words: X-rays: general – Galaxies: individual: M31 – X-rays: binaries – Accretion: accretion discs – Methods: numerical

1 INTRODUCTION

Bo 158 is source number 158 in the catalogue of globular clusters that were identified in M31 by Battistini et al. (1987). Its X-ray counterpart was discovered by the Einstein Observatory (Trinchieri & Fabbiano 1991, source number 81), and is located at $\alpha = 00^{\text{h}}43^{\text{m}}14.2^{\text{s}}$, $\delta = 41^{\circ}07'26.3''$ (Di Stefano et al. 2002). Trudolyubov et al. (2002) identified the X-ray source as a likely low mass X-ray binary (LMXB) with a neutron star primary; following their work, we will use the designation “Bo 158” to describe the X-ray source here.

Trudolyubov et al. (2002) report $\sim 83\%$ modulation in the 0.3–10 keV flux of Bo 158 on a 2.78 hour period during the ~ 60 ks 2002 January XMM-Newton observation. The modulation resembles the intensity dips seen in high inclination LMXBs due to photo-electric absorption of X-rays by material that is raised above the body of the accretion disc (White & Swank 1982). The authors comment that the dipping is energy-independent, and discuss two possible mechanisms: obscuration of the central X-ray source by highly

ionised material that scatters X-rays out of the line of sight, and the partial covering of an extended source by an opaque absorber. They also report $\sim 30\%$ dips in the 2000, June XMM-Newton lightcurve and $\sim 50\%$ dips in the 0.2–2.0 keV lightcurve of the 1991, June 26 ROSAT/PSPC observation. However, no significant dips were found in the 0.3–10 keV lightcurve of the 2001 June XMM-Newton observation; the authors placed a 2σ upper limit of 10% on the modulation.

Trudolyubov et al. (2002) obtained fluxes in the 0.3–10 keV band for the three XMM-Newton observations by fitting absorbed Comptonisation models to the combined spectra of the EPIC-pn, MOS1 and MOS2, and concluded that the depth of the intensity modulation was anti-correlated with the source luminosity. We present further XMM-Newton observations and modelling results which suggest that the variation in dipping behaviour may instead be due to precession in the accretion disc. Such behaviour is associated with the “superhump” phenomenon that is observed in interacting binaries where the mass ratio of the secondary to the primary is smaller than ~ 0.3 (Whitehurst & King 1991). Superhumps are briefly reviewed in Sect. 2, followed by details of the observations and data analysis in Sect. 3, and our results in Sect. 4. Numerical modelling of the system

* Email address: R.Barnard@open.ac.uk

is discussed in Sect. 5; the system was simulated by a 3D smoothed particle hydrodynamics (SPH) code. We present our discussion in Sect. 6, and finally our conclusion in Sect. 7.

2 SUPERHUMPS

Superhumps were first identified in the superoutbursts of the SU UMa sub-class of cataclysmic variables. They are manifested as a periodic increase in the optical brightness on a period that is a few percent longer than the orbital period (Vogt 1974; Warner 1975). SU UMas are a subclass of dwarf novae with short orbital periods ($\lesssim 2$ hr) that exhibit particularly long, bright superoutbursts, separated by several outbursts that are typical of all dwarf novae; the superoutburst intervals are $\gtrsim 5$ times longer than the normal outbursts. (Vogt 1980).

In the model proposed by Osaki (1989), a superoutburst is occurs when a normal outburst is enhanced by a tidal instability; this occurs when the outer disc reaches a 3:1 resonance with the secondary. The disc is small at the start of the superoutburst cycle, well within the radius of tidal instability, and little angular momentum is removed by tidal interaction during the first normal outburst. Hence, the disc cannot accrete all of its mass onto the neutron star, and the size of the disc increases with successive outbursts, until the 3:1 resonance is reached (Osaki 1989). The additional tidal forces exerted on the disc by the secondary at this stage cause the disc to elongate and precess, and also greatly enhance the loss of angular momentum, so that the disc contracts, and most of the disc material is snow-ploughed onto the neutron star, causing the superoutburst (Osaki 1989). The disc precession is prograde in the rest frame, and the secondary repeats its motion with respect to the disc on the beat period between the orbital and precession periods, slightly longer than the orbital period. The secondary modulates the disc's viscous dissipation on this period, giving rise to maxima in the optical lightcurve, known as superhumps.

The requirement for the 3:1 resonance to fall within the disc's tidal radius is that the mass ratio of the secondary to the primary be less than ~ 0.33 (Whitehurst & King 1991). If we assume that the secondary is a main sequence star that fills its Roche lobe, then the relation $m_2 \simeq 0.11 P_{\text{hr}}$ holds, where m_2 is the mass of the secondary in solar units and P_{hr} is the orbital period in hours (e.g. Frank, King & Raine 2002). Hence any accreting binary that has a short enough orbital period may exhibit superhumps. Indeed, there exists a class of short-period, persistently bright CVs that exhibit permanent superhumps (Patterson 1999; Retter & Naylor 2000).

Haswell et al. (2001) discuss analogous superhump behaviour in LMXBs. Although superhumps have been found in the optical lightcurves of several black hole and neutron star LMXBs, they cannot be produced by the same mechanism, since the optical output of X-ray bright LMXBs is dominated by reprocessed X-rays. Instead, Haswell et al. (2001) proposed that the modulation is due to variation of the solid angle that the disc subtends to the X-ray source (on the superhump period); in this model, superhumping might be expected to be more prominent in low inclination systems.

4U 1916–053 is a neutron star LMXB, with an X-

Table 1. Journal of XMM-Newton observations of the M31 core. A1–A3 are available in the public archive, while P4–P6 are proprietary observations. Two observations were made during 2004 July 19; the first observation (a) started at 01:42:12, and the second (b) started at 13:11:22.

Observation	Date	Exp	Filter
A1	2000 Jun 25	34 ks	Medium
A2	2001 Jun 29	56 ks	Medium
A3	2002 Jan 6	61 ks	Thin
P4	2004 Jul 17	18 ks	Medium
P5	2004 Jul 19a	22 ks	Medium
P6	2004 Jul 19b	27 ks	Medium

ray period of 50.00 min and an optical period of 50.4589 min (Callanan et al. 1995). Haswell et al. (2001) show that LMXBs with orbital periods shorter than ~ 4.2 hr are likely to exhibit superhumps, and identified 4U 1916–053 as a persistent irradiated superhumping source. 4U 1916–053 is a high inclination system, with periodic intensity dips in the X-ray lightcurve (White & Swank 1982). These dips are due to photo-electric absorption by material on the outer edge of the accretion disc; many believe that the inflated bulge on the outer disc rim that is caused by the collision between the gas stream and the outer disc is responsible (see e.g. White & Holt 1982). The X-ray modulation of 4U 1916–053 shows striking variability (Smale et al. 1988). These variations repeat on a ~ 4 day period, and are caused by the precession of the accretion disc (see e.g. Chou et al. 2001). When Retter et al. (2002) made power density spectra (PDS) of the X-ray lightcurve of 4U 1916-05, they found peaks corresponding to both the X-ray and optical periods. After removing the dipping intervals, the optical peak was removed; hence the dips were shown to occur on the superhump period. Retter et al. (2002) concluded that the observed superhumps arose from the same thickened region of the outer disc that caused the absorption of the X-rays, allowing superhumps to be seen in high inclination LMXBs.

3 OBSERVATIONS AND DATA ANALYSIS

In addition to the three XMM-Newton observations analysed by Trudolyubov et al. (2002), we conducted a programme of four ~ 20 ks observations over 2004, July 16–19. We present results from our analysis of the archival data, along with three of the four 2004 observations; the other observation suffered from flaring in the particle background over 90% of the observation and is not considered further here. A journal of observations is presented in Table 1.

We analysed data from the pn, MOS1 and MOS2 instruments, which share the same $30'' \times 30''$ field of view. We used version 6.0.0 of the *SAS* software suite¹ to obtain the data products, as well as the latest calibration data. For each observation, we selected a circular extraction region with a $40''$ radius, centred on Bo 158, and an equivalent source-free region for the background. The background region was on

¹ <http://xmm.vilspa.esa.es>

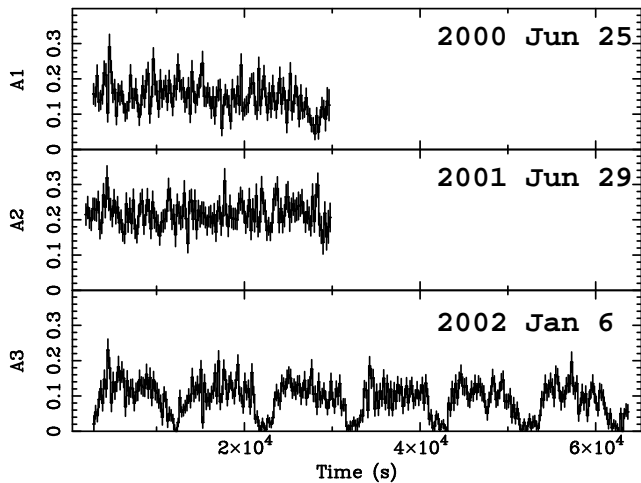


Figure 1. Combined EPIC 0.3–10 keV lightcurves (in count s^{-1}) of Bo 158 from the archival XMM-Newton observations, A1–A3; the dates of each observation are shown.

the same chip as the source, and at a similar angular offset from the optical axis. We extracted lightcurves from the source and background regions in the 0.3–10 keV, 0.3–2.5 keV and 2.5–10 keV energy bands with 2.6 s binning; these were analysed using *FTOOLS* version 5.3.1. We also obtained pn spectra of the source and background regions in 4096 channels of 5 eV, and generated response matrix and ancillary response files from the source spectral files. The spectra were then grouped for a minimum of 50 counts per bin. Spectral analysis was performed using *XSPEC* 11.3.1.

4 RESULTS

The 0.3–10 keV EPIC (MOS1 + MOS2 + pn) lightcurves of Observations A1–A3 are presented in Fig. 1, with x- and y-axes set to the same scale, and with 200 s binning. Most striking is Observation A3, with six dipping intervals on a 10017 ± 50 second period (Trudolyubov et al. 2002); the structure of the dipping is seen to vary substantially even over one observation of 60 ks. We emphasise that the 30% dipping reported by Trudolyubov et al. (2002) for observation A1 is an overall average; a deep dip is seen at ~ 28 ks into the observation, but very little evidence of dipping is observed in the intervals of expected dipping at ~ 8 ks and ~ 18 ks into the observation. In this regard, Observation A1 resembles the 1985, October lightcurve of 4U 1916–053, observed by EXOSAT, where deep dips were observed only after the first four orbital cycles (Smale et al. 1988). Little evidence of variability is seen in the lightcurve of Observation A2.

In Fig. 2, we present the 0.3–10 keV EPIC lightcurves of Observations P4–P6; the x-axis is scaled to P6, and the y-axis matches that of Fig. 1. The most prominent feature is the dip in P5; it has a depth of $\sim 100\%$ and a total duration of ~ 2500 s. Using the period of Trudolyubov et al. (2002), we identified the expected times of dipping, labelled ‘D’, in P4 and P6, using the deepest part of the dip in P5 as phase zero.

In the P4 lightcurve, there is no evidence for dipping during the first expected dip interval, but some evidence of

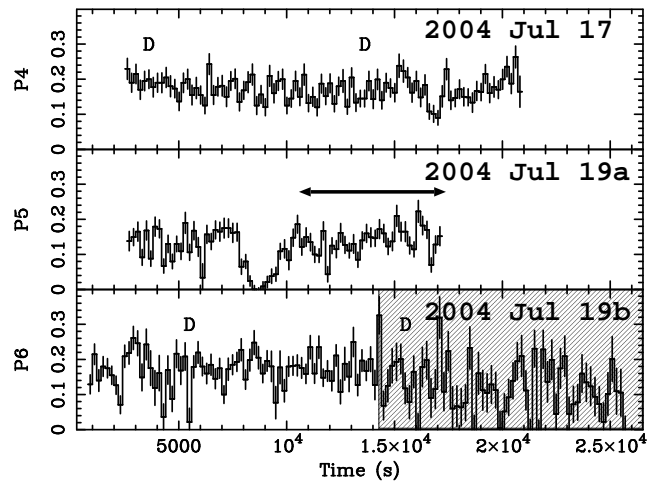


Figure 2. Combined EPIC 0.3–10 keV lightcurves (in count s^{-1}) of Bo 158 from the 2004 XMM-Newton observations, P4–P6; the dates of each observation are shown. The horizontal line in the P5 lightcurve indicates the interval used for spectral fitting. The shaded area of the P6 lightcurve indicates a period of background flaring. Times when dipping is expected are labelled ‘D’, using the deepest part of the dip in P5 as time zero, and the period of Trudolyubov et al. (2002).

dipping ~ 4000 s after the second interval, 20 cycles away from the dip in P5. Hence, this possible dip would require a period that is either ~ 200 s shorter or ~ 320 s longer than the 10017 s given by Trudolyubov et al. (2002). However, there is no other evidence for these other periods in the lightcurves of P4, P5 or P6; hence it is clear that the dipping behaviour of Bo 158 evolves on a time scale of a few days, just like that of 4U 1916–053.

Several emission models were fitted to the 0.3–10 keV pn spectrum of P4, each suffering absorption by material in the line of sight. P4 was chosen because it had the longest interval of persistent emission that was not contaminated by background flares; the resulting source spectrum contained ~ 2200 counts. We applied the two models that Trudolyubov et al. (2002) used to model the spectra of A1–A3, namely a power law model and a Comptonisation model (COMPTT in XSPEC). We also applied a two component model. The emission of many Galactic LMXBs has been successfully described by a model consisting of a blackbody and a cut-off power law (e.g. Church & Bałucińska-Church 1995; Church et al. 1998; Barnard et al. 2003); we approximate this model to a blackbody + power law model, because of the narrow pass-band. Table 2 shows the best fits to the spectrum with each model; uncertainties are quoted at the 90% confidence level.

We find that the best fit parameters for the power law and COMPTT models agree well with the values presented by Trudolyubov et al. (2002); however, the two-component model provided the best fit. We present the unfolded SED for the two component fit in Fig. 3; the emission from the blackbody (BB) and power law (PO) components are shown separately. We see that the blackbody dominates the emission above 1.5 keV. We find a 0.3–10 keV flux of $\sim 2 \times 10^{-12}$ erg cm^{-2} s^{-1} for all the fits to the P4 data; this gives a 0.3–10 keV luminosity of $\sim 1.4 \times 10^{38}$ erg s^{-1} , assuming a distance of 760 kpc (van den Bergh 2000).

Table 2. Best fits to the P4 (2004 July 16) pn spectrum of Bo 158 for several emission models; these are power law (PO), Comptonisation (COMP TT), and blackbody + power law (BB+PO) models, suffering line-of-sight absorption by the interstellar medium. N_{H} is the equivalent hydrogen column density of the absorber, T_0 is the seed photon temperature (COMP TT), T is the blackbody temperature (COMP TT, BB+PO), τ is the optical depth (COMP TT) and Γ is the photon index (PO, BB+PO). The goodness of fit is given by χ^2/dof , and $F_{0.3-10}$ is the unabsorbed flux in the 0.3–10 keV band.

Model	N_{H} atom cm $^{-2}$	kT_0 keV	kT keV	τ	Γ	χ^2/dof	$F_{0.3-10}$ 10^{-12} erg cm 2 s $^{-1}$
PO	0.1	0.57 \pm 0.09	30/24	2.3 \pm 0.3
COMP TT	0.1	0.08 \pm 0.07	2.4 \pm 0.6	17 \pm 2	...	22/19	2.2 $^{+0.2}_{-2.0}$
BB+PO	0.1	...	2.0 \pm 0.2	...	2.0 \pm 0.3	19/19	2.1 \pm 0.8

We then extracted the SED from the interval of \sim persistent emission in P5 indicated in Fig. 3 by a horizontal line. The resulting background-subtracted SED contained 452 counts in the 0.3–10 keV band, which we divided into 10 spectral bins. The spectral shape of the P5 SED was consistent with that of P4, with a luminosity of $1.2 \pm 0.2 \times 10^{38}$ erg s $^{-1}$. Hence the luminosity of persistent emission in P5 is consistent with that of P4 within 3σ .

The depth of dipping in A1 varies from ~ 0 to $\sim 70\%$ with no significant change in the mean intensity, suggesting that the amplitude of dipping is not simply anticorrelated with the source luminosity. Instead, the variation in dipping behaviour may be caused by disc precession. This hypothesis motivated our simulation of the accretion disc in Bo 158, using three dimensional smoothed partial hydrodynamics, discussed in Sect. 5.

The lightcurves of XMM-Newton observations of Bo 158 show no eclipses; hence, we know that we are not viewing the system edge on. If the disc were tilted with respect to the binary plane, and precessing, then one might expect to observe dips in some part of the disc precession cycle, but not in others. Dipping is observed throughout observation A3; this suggests that the dipping phase in the disc precession cycle lasts $\gtrsim 60$ ks. The A1 lightcurve covered three intervals of expected dipping, yet only one dip is seen, toward the end of the observation; we suggest that this dip signals the onset of the dipping phase. Contrariwise, P5 and P6 appear to sample the end of the dipping phase, as a dip is observed in P5, yet no dips are seen in P6.

5 SPH SIMULATION OF THE DISC

5.1 Binary Parameters

The accretion disc was modelled using a three-dimensional Smoothed Particle Hydrodynamics (SPH) computer code that has been described in detail in Murray (1996, 1998), Truss et al. (2000), and Foulkes, Haswell & Murray (2005). We assumed the orbital period to be 10017 s, as obtained by Trudolyubov et al. (2002). Table 3 lists the system parameters adopted.

The dipping source Bo 158 is a bright globular cluster X-ray source, with a 2.78 hr binary period. Thirteen Galactic globular clusters contain bright X-ray sources; twelve of these are neutron star LMXBs, while the primary of the other one is unknown (see e.g. in't Zand et al. 2004). Hence

Bo 158 is a likely neutron star LMXB, and we assume the primary mass to be $1.4 M_{\odot}$.

For the secondary, we considered a main sequence star and a white dwarf, since 4U 1916–053 has a likely white dwarf secondary (e.g. Chou et al. 2001). For a Roche lobe-filling main sequence star the approximate relation $m \simeq 0.11 P_{\text{hr}}$ holds (e.g. Frank et al. 2002), giving a mass of $\sim 0.30 M_{\odot}$. If instead the star is a white dwarf, using the mass radius relation of Nauenberg (1972) and Roche geometry gives an implausibly small mass of $0.005 M_{\odot}$. Assuming a main sequence secondary, we found the mass ratio to be 0.2, indicating that superhumps and disc precession were likely.

Finally, the luminosity of the system was taken to be 1.4×10^{38} erg s $^{-1}$, the 0.3–10 keV luminosity of Bo 158 in Observation P4. Such a high luminosity may be expected to cause warping of the accretion disc, even for a previously flat disc (see e.g. Pringle 1996); warping is discussed in Sect. 5.3.

The accretion disc had an open inner boundary condition in the form of a hole of radius $r_1 = 0.025a$, where a is the binary separation, centred on the position of the primary object. Particles entering the hole were removed from the simulation. Particles that re-entered the secondary Roche lobe were also removed from the simulation as were particles that were ejected from the disc at a distance $> 0.9a$ from the centre of mass.

We assumed an isothermal equation of state and that the dissipated energy was radiated from the point at which it was generated, as electromagnetic radiation. The Shakura & Sunyaev (1973) viscosity parameters were set to $\alpha_{\text{low}} = 0.1$ and $\alpha_{\text{high}} = 1.0$, and the viscosity state changed smoothly as described in Truss et al. (2000). The SPH smoothing length, h , was allowed to vary in both space and time and had a maximum value of $0.01a$.

5.1.1 The gas stream

We simulated the mass loss from the secondary by introducing particles at the inner Lagrangian point (L_1). The mass transfer rate and the particle transfer rate were provided as input parameters, and the mass of each particle was derived from these parameters. A particle was inserted with an initial velocity (in the orbital plane) equal to the local sound speed of the donor, c_{D} , in a direction prograde of the binary axis. The z velocity of the inserted particle was chosen from a Gaussian distribution, with a zero mean and a variance of

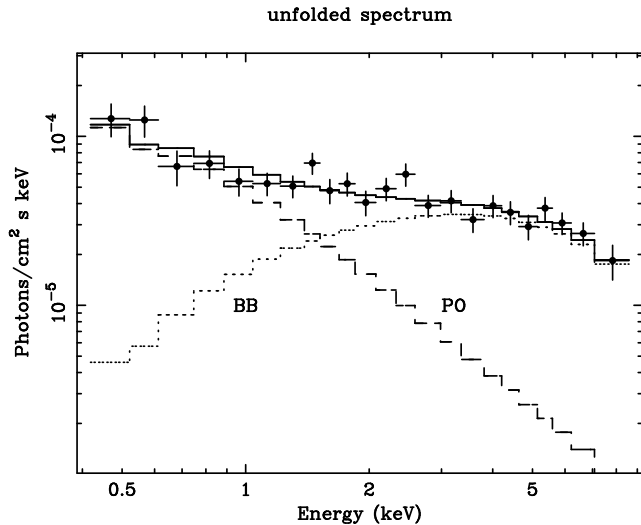


Figure 3. Unfolded EPIC-pn SED of Bo 158 from observation P4, described by the best fit two component model. The dotted line represents the blackbody component (BB), while the dashed line shows the power law component (PO). The solid line shows the sum of the two components. The blackbody component dominates the flux above 1.5 keV.

$0.1c_D$. However, the inflation of the site of collision between the gas stream and outer disc was not modelled.

5.1.2 The initial non-warped accretion disc

The simulation was started with zero mass in the accretion disc and with the central radiation source switched off. A single particle was injected into the simulation every $0.01\Omega_{orb}^{-1}$ at the L_1 point as described above until a quasi-steady mass equilibrium was reached within the disc. This was taken to be when the number of particles inserted at the L_1 point, the mass transfer rate, was approximately equal to number of particles leaving the simulation at the accretor, the accretion rate. The simulations were continued for another 3 orbital periods to ensure mass equilibrium. The number of particles in the simulated accretion disc was approximately 40,000 giving a good spatial resolution; the average number of ‘neighbours’, i.e. the average number of particles used in the SPH update equations, was 8.2 particles. The simulated disc encountered the Lindblad 3:1 resonance and became eccentric. The disc precessed in a prograde direction giving rise to superhumps in the simulated dissipation light-curves (c.f. Foulkes et al. 2004). The radiation source was then turned on which gave rise to a very small number of particles being ejected from the accretion disc.

5.2 Surface finding algorithm & self-shadowing

Accretion-powered radiation from the inner regions of the disc and the accreting object itself exert a force on the irradiated disc surface. Following Pringle (1996) the radiation source is modelled as a point source at the centre of mass of the accretor. To apply this force, particles on the surface of the accretion disc had to be identified. We used a convex hull algorithm to find the surface particles as described in Murray (1998) and Foulkes et al. (2005). A ray-tracing algo-

rithm was used to determine regions of self-shadow. For each particle found on the disc surface a light-ray was projected from the particle to the position of the radiation source at the centre of the disc. The particle was deemed to be illuminated by the radiation source if this light-ray did not intersect any disc material between the particle surface position and the radiation source (i.e. the particle could see the central radiation source). The radiation force was only applied to particles that were considered to form part of the disc surface and were illuminated by the central radiation source.

5.3 Disc warping and precession measure

For an optically thick disc, a warp can develop as a result of the radiation force (e.g. Pringle 1996; Ogilvie & Dubus 2001; Foulkes et al. 2005). This is due to the fact that any radiation absorbed by a specific region on the disc surface will be later re-radiated from the same spot, normal to the disc surface. Hence any anisotropy in the disc structure will cause an uneven distribution of back-reaction forces on the disc surface, further perturbing the disc. A sufficiently high luminosity can induce and sustain a warp even in an originally flat disc (Pringle 1996, and references therein).

The two measures defined by Larwood & Papaloizou (1997) were used to measure the disc warping and the amount of warp precession. They defined an angle j as the angle between the total disc angular momentum vector and the angular momentum vector for a specific disc annulus, i.e.

$$\cos j = \frac{\mathbf{J}_A \cdot \mathbf{J}_D}{|\mathbf{J}_A| |\mathbf{J}_D|}. \quad (1)$$

The term \mathbf{J}_A is the total angular momentum within the specific annulus and was calculated by summing the angular momentum for each particle within the annulus. The term \mathbf{J}_D is the total disc angular momentum and was calculated by summing all the angular momenta for all particles within the disc. An angle Π was also defined which measures the amount of precession of the disc angular momentum relative to the initial binary orbital angular momentum, \mathbf{J}_O

$$\cos \Pi = \frac{(\mathbf{J}_O \times \mathbf{J}_D) \cdot \mathbf{u}}{|\mathbf{J}_O \times \mathbf{J}_D| |\mathbf{u}|} \quad (2)$$

where \mathbf{u} is any arbitrary vector in the binary orbital plane.

5.4 Numerical modelling results

Prior to irradiation, the disc was asymmetric about the binary axis and precessed in a prograde direction relative to the inertial frame. After switching the radiation source on we ran the model for a further 50 orbital periods, and found that this illumination introduced a warp in the disc. When the radiation source was removed, the warp would dissipate and the disc would return to the orbital plane.

As a result of the disc precession, viscous stresses in the disc vary significantly with time. Figure 4 shows how the resultant energy dissipation in different regions of the disc varies with time. The disc luminosity was not modelled in detail. We assume that the luminosity was directly related to the disc regions with significant energy release through

Table 3. Binary system parameters for the system modelled. The columns are: the total system mass, the system orbital period, the rate of mass loss from the secondary, the system mass ratio, the physical luminosity of the central radiation source and the ratio of the physical luminosity to the Eddington limit for the system.

Parameter	M_t M_\odot	P_{orb} <i>days</i>	\dot{M}_{sec} $M_\odot yr^{-1}$	q (M_2/M_1)	Physical luminosity (L_*) ($erg\ s^{-1}$)	L_*/L_{edd}
Value	1.8	0.1159	2.22×10^{-8}	0.2	1.4×10^{38}	0.8

viscous dissipation. The viscous dissipation heats the gas in the accretion disc and it is assumed that the heat is radiated away from the point at which it was generated. Superposed on a steady signal there is a repeating series of ‘‘humps.’’ The spacing of the humps corresponds to the superhump period. The humps consist of three separate major components. The maximum occurs at phase ~ 0.2 , followed by a secondary maximum at phase ~ 0.5 , and the minimum at ~ 0.7 ; however the relative strengths of the humps vary from cycle to cycle. We stress that the dissipation lightcurves are only a diagnostic for the disc properties, i.e. for identifying the the superhumps, as well as the intervals when the disc structure is most extended or most compressed. They are not representative of true optical lightcurves.

In order to determine the superhump period, P_{sh} , we obtained a power density spectrum from ~ 30 superhump cycles of the simulated light curve. We estimated the superhump period to be $(1.035 \pm 0.005)P_{orb}$. This implies the precession period of the outer regions, $P_{prec} = (29 \pm 1)P_{orb}$, or 81 ± 3 hr.

Fig. 5 contains projection plots for the time period corresponding to the peak labelled ‘‘max1’’ in Fig. 4, at phase ~ 2.2 . A very strong spiral density compression wave can be seen at the upper edge of the disc. This wave is so intense that it is removing material from the accretion disc and returning it back to the Roche lobe of the secondary, see Foulkes et al. (2004) for a full detailed description of a similar system with a mass ratio of 0.1.

The two upper right-hand plots of Fig. 5, labelled yz-view and xz-view, are side views of the disc in the y-z and x-z directions respectively. The yz-view plot is a projection view of the disc as seen from the secondary, similarly the xz-view is a projection plot with the secondary located to the right of the plot. The disc warp is clearly apparent in these two plots. The warp is odd symmetrical about the centre of the disc. The maximum value of the warp is located at a distance approximately $0.1a$ either side of the primary position, see yz-view of Fig. 5.

The lower plot of Fig. 5, labelled accretor-view, shows the distribution of the particles as seen from the compact object. The horizontal axis is the binary orbital phase, L_1 is located at phase 0 and disc material flows from right to left with the stream-disc impact region located at approximately phase 0.9. The vertical axis is the elevation angle of the particle as seen from the primary position. From this plot it can be seen that the radiation force has pushed disc material out of the orbital plane. The warp reaches a maximum height above the orbital plane at phases ~ 0.1 and ~ 0.6 , and has minima at phases ~ 0.45 and ~ 0.95 . We also see that the

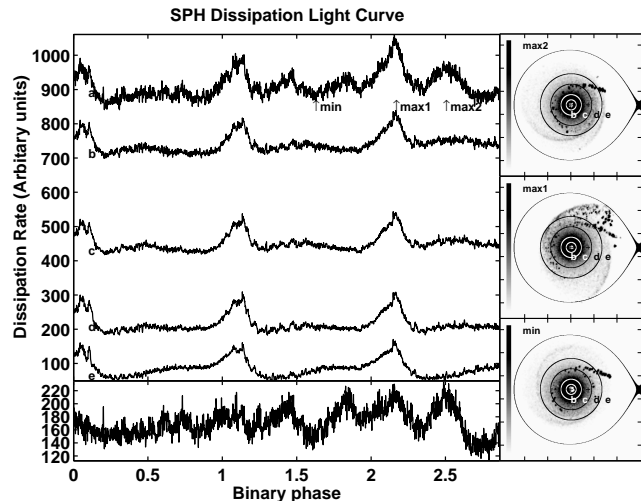


Figure 4. The top left plot shows SPH viscous dissipation light curves for different regions of the accretion disc. The top curve, labelled *a*, is for the whole accretion disc, then each curve in descending order corresponds to dissipation in the disc at radii $> 0.05a(b)$, $> 0.1a(c)$, $> 0.2a(d)$ and $> 0.3a(e)$ respectively. The light curve minimum and two maximum points are indicated. The lower left-hand plot is the signal from the disc inner region and was generated by subtracting light curve *b* from light curve *a*. The plots on the right-hand side are disc dissipation maps that correspond to the light curve minimum and two maxima. The circles labelled *b*, *c*, *d* and *e* show the distances from the primary that correspond to the light curves *b*, *c*, *d*, *e* respectively.

disc remains mainly in the orbital plane, although it can be seen that there is a small S-wave in the structure of the disc.

The warp amplitude and size precessed as a solid body in a retrograde direction relative to the inertial frame. The warp precession period, P_{warp} , was determined by applying equation (2) to each time step of the simulation. This gave a precession angle relative to some arbitrary start angle for each simulation time step. The warp precession rate was then determined by fitting a straight line to these data using a Numerical Recipes least squares method, (Press et al. 1986). The precession rate was found using the gradient of the line extracted from the least squares fit. We found that $P_{warp} \sim 11 P_{orb}$. Figure 6 shows the radial profile of the warp for five consecutive orbital cycles; the maximum extent of the warp is $6\text{--}11^\circ$ above the plane of the disc.

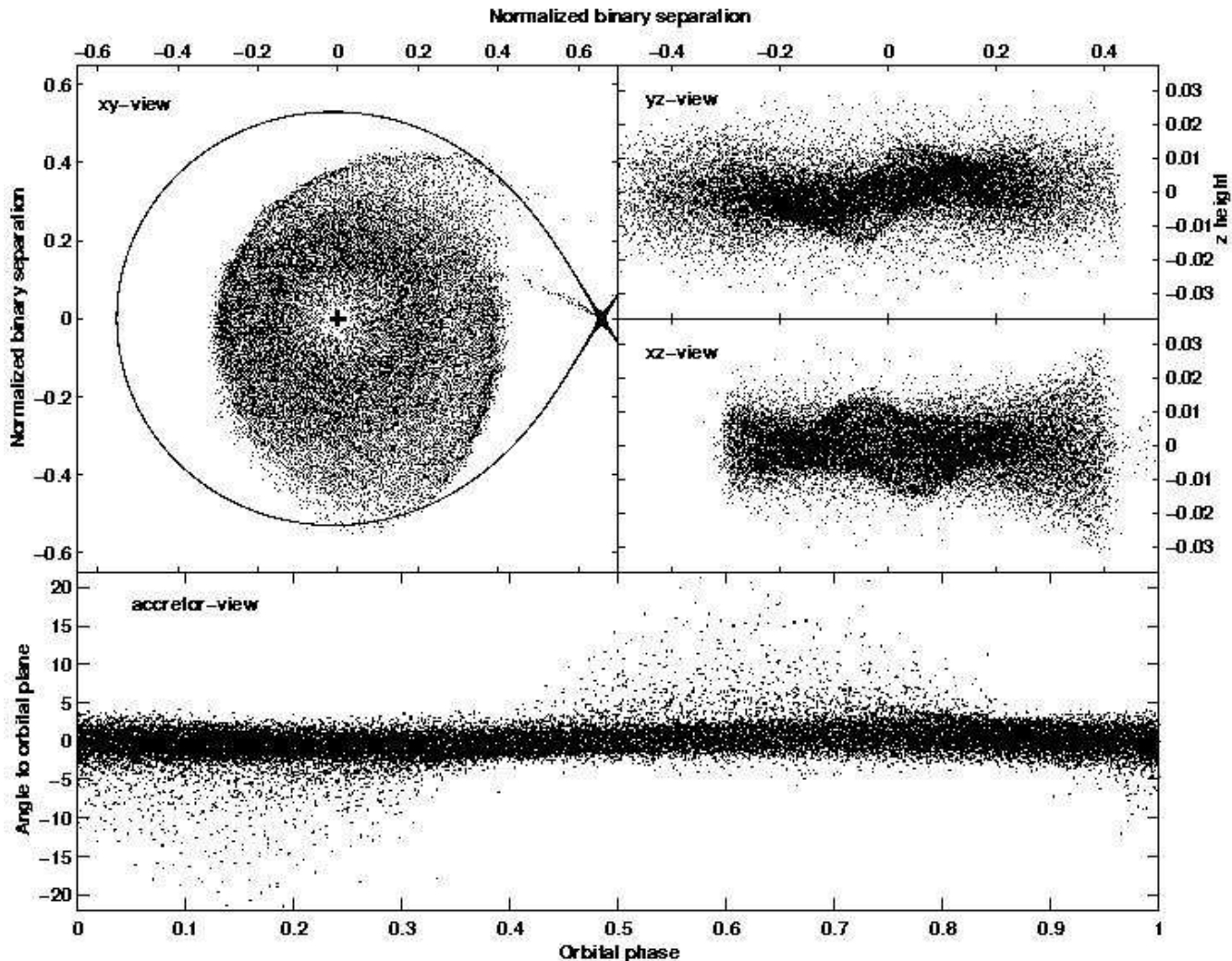


Figure 5. Particle projection plots for the SPH model. The position of each particle is indicated by a small black dot. The plot labelled *xy-view* is a plan view of the accretion disc as seen from above the disc. The cross at the centre of the plot shows the position of the primary object. The solid dark line is the Roche lobe of the primary and the L_1 point is to the right and middle of the plot. The two plots *xz-view* and *yz-view* are particle projection plots on a plane perpendicular to the orbital plane and through the system axis. The bottom plot, *accretor-view*, shows the particle distribution as seen from the compact object. The horizontal axis is the orbital phase, the L_1 point is at phase 0 and the stream/disc impact region is at approximately phase 0.9. The vertical axis is the angle, in degrees, between a particle and the orbital plane when viewed from the compact object. The disc material flows from right to left.

6 DISCUSSION

We report a single $\sim 100\%$ dip in the 0.3–10 keV EPIC lightcurve of Bo 158 from Observation P5, but find little evidence of dipping in Observations P4 and P6. Trudolyubov et al. (2002) propose two models to explain the energy independence of dipping that they inferred from Bo 158: (1) absorption by a highly ionised region and (2) partial covering of an extended source by an opaque absorber that occults varying fractions of the source. However, in their figure showing both non-dip and dip SEDs, the two SEDs converge at high energies, showing that the dipping is indeed energy dependent.

The dipping behaviour of many Galactic LMXBs has been well described by a single model: absorption of a point-like blackbody plus progressive covering of an extended emission region by an extended absorber (Church et al.

1997). This extended emission is caused by unsaturated inverse-Comptonisation of cool photons on hot electrons in an accretion disc corona that has a radius of $\sim 10,000$ – $500,000$ km (Church & Bałucińska-Church 2004). The saturated dipping exhibited by 4U 1624–490 during a 1985 EXOSAT observation is particularly strong evidence for an extended absorber (Church & Bałucińska-Church 1995). The 0.1–200 keV observations of 4U 1916–053 with Beppo-SAX have shown that the absorber is so dense that $\sim 100\%$ photoelectric absorption occurs up to 10 keV; in fact, the dipping is seen up to 40 keV (Church et al. 1998). However, the high luminosity of Bo 158, together with the large blackbody contribution, mean that the dipping is unlikely to be energy-independent.

Disc precession is inferred from the 0.3–10 keV lightcurves of Bo 158, as is expected given its extreme mass ratio (short orbital period). As such, it resembles the Galac-

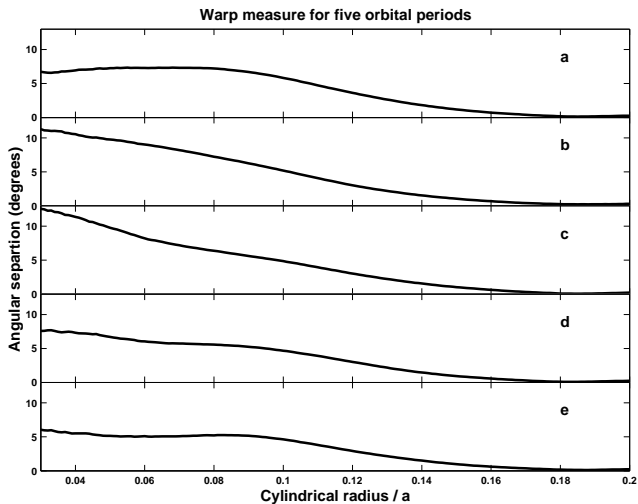


Figure 6. Radial warp profiles evaluated using equation (1). The vertical axis is the warp amplitude. The horizontal axis is distance from the primary object normalized such that the binary separation is 1. Plots (a), (b), (c), (d) and (e) are for five consecutive orbital cycles.

tic superhumping LMXB 4U 1916–053. Since the LMXB Bo 158 is in a globular cluster near the centre of M31, it is unlikely that the optical period will ever be known. However, our Fourier analysis of the simulated dissipation lightcurves indicates a superhump period that is $3.5 \pm 0.5\%$ longer than the orbital period. Given the association between the dips and superhump period reported by Retter et al. (2002), the 10017 s period may be the superhump period, in which case, the orbital period would be $\sim 4\%$ shorter. Such shortening of the period would not dramatically affect the outcome of our SPH modelling.

Our simulations of the disc show two distinct types of variability in the disc structure. First is the elongation and prograde precession of the disc due to tidal interactions with the secondary at the 3:1 resonance; the disc precesses on period of 81 ± 3 hr. We also see warping of the accretion disc, driven by irradiation of the disc surface by the central X-ray source; the warp is stable exhibits retrograde precession on a ~ 31 -hr period.

It is therefore important to establish which region is responsible for the observed variation in dip morphology. The lightcurves of observations A1–P6 show no eclipses. From Kepler’s law and the ratio of the secondary ratio to the binary separation (Eggleton 1983), the secondary has an angular radius of $\sim 15^\circ$; hence the inclination $\lesssim 75^\circ$. We see from Fig. 6 that the disc warp does not deviate from the plane of the disc by more than 11° in our simulations, suggesting that the observed dips are likely to evolve on the disc precession period.

7 CONCLUSIONS

We have analysed three new XMM-Newton observations of the M31 dipping LMXB Bo 158, in addition to re-analysing the three observations discussed in Trudolyubov et al. (2002). The newer observations spanned ~ 3 days in 2004, July. We find that that the relationship between source in-

tensity and depth of dipping is not simple, as described by Trudolyubov et al. (2002). Instead, we believe that the observed variation in dipping behaviour is caused by precession in the accretion disc; dipping would be confined to a limited phase range in the disc precession cycle.

We modelled the accretion disc with 3D SPH, and found prograde disc precession on a 81 ± 3 hr period, as well as radiatively driven disc warp that precessed on a 31 hr period in a retrograde fashion. We find that the disc precession is most likely to affect the observed dipping behaviour. Hence, we predict that the dipping behaviour of Bo 158 experiences a 81 ± 3 hour cycle; this period is consistent with the observed variation of the dips.

ACKNOWLEDGMENTS

We would like to thank the anonymous referee for their constructive comments. R.B. gratefully acknowledges support from PPARC.

REFERENCES

- Barnard R., Church M. J., Bałucińska-Church M., 2003, *A&A*, 405, 237
- Battistini P., Bonoli F., Braccesi A., Federici L., Fusi Pecci F., Marano B., Borngen F., 1987, *A&AS*, 67, 447
- Callanan P. J., Grindlay J. E., Cool A. M., 1995, *PASJ*, 47, 153
- Chou Y., Grindlay J. E., Bloser P. F., 2001, *ApJ*, 549, 1135
- Church M. J., Bałucińska-Church M., 1995, *A&A*, 300, 441
- Church M. J., Bałucińska-Church M., 2004, *MNRAS*, 348, 955
- Church M. J., Dotani T., Balucinska-Church M., Mitsuda K., Takahashi T., Inoue H., Yoshida K., 1997, *Apj*, 491, 388
- Church M. J., Parmar A. N., Balucinska-Church M., Oosterbroek T., dal Fiume D., Orlandini M., 1998, *A&A*, 338, 556
- Di Stefano R., Kong A. K. H., Garcia M. R., Barmby P., Greiner J., Murray S. S., Primini F. A., 2002, *ApJ*, 570, 618
- Eggleton P. P., 1983, *ApJ*, 268, 368
- Foulkes S. B., Haswell C. A., Murray J. R., Rolfe D. J., 2004, *MNRAS*, 349, 1179
- Foulkes S. F., Haswell C. A., Murray J. R., 2005
- Frank J., King A. R., Raine D., 2002, *Accretion Power in Astrophysics*, 3rd Edition. Cambridge University Press
- Haswell C. A., King A. R., Murray J. R., Charles P. A., 2001, *MNRAS*, 321, 475
- in’t Zand J., Verbunt F., Heise J., Bazzano A., Cocchi M., Cornelisse R., Kuulkers E., Natalucci L., Ubertini P., 2004, To appear in “The Restless High-Energy Universe” (2nd BeppoSAX Symposium), eds. E.P.J. van den Heuvel, J.J.M. in ’t Zand & R.A.M.J. Wijers, *Nucl. Instrum. Meth. B Suppl. Ser.*, astro-ph/0403120
- Larwood J. D., Papaloizou J. C. B., 1997, *MNRAS*, 285, 288
- Murray J. R., 1996, *MNRAS*, 279, 402
- Murray J. R., 1998, *MNRAS*, 297, 323
- Nauenberg M., 1972, *Apj*, 175, 417

- Ogilvie G. I., Dubus G., 2001, MNRAS, 320, 485
Osaki Y., 1989, PASJ, 41, 1005
Patterson J., 1999, in Disk Instabilities in Close Binary Systems Permanent Superhumps in Cataclysmic Variables. pp 61–+
Press W. H., Flannery B. P., Teukolsky S. A., 1986, Numerical recipes. The art of scientific computing. Cambridge: University Press, 1986
Pringle J. E., 1996, MNRAS, 281, 357
Retter A., Chou Y., Bedding T. R., Naylor T., 2002, MNRAS, 330, L37
Retter A., Naylor T., 2000, MNRAS, 319, 510
Shakura N. I., Sunyaev R. A., 1973, A&A, 24, 337
Smale A. P., Mason K. O., White N. E., Gottwald M., 1988, MNRAS, 232, 647
Trinchieri G., Fabbiano G., 1991, ApJ, 382, 82
Trudolyubov S., Borozdin K. N., Priedhorcky W. C., Osborne J. P., Mason K. O., Cordova F. A., 2002, ApJL, 581, L27
Truss M. R., Murray J. R., Wynn G. A., Edgar R. G., 2000, MNRAS, 319, 467
van den Bergh S., 2000, The galaxies of the Local Group, Cambridge University Press, Cambridge Astrophysics Series, vol no: 35
Vogt N., 1974, A&A, 36, 369
Vogt N., 1980, A&A, 88, 66
Warner B., 1975, MNRAS, 170, 219
White N. E., Holt S. S., 1982, ApJ, 257, 318
White N. E., Swank J. H., 1982, ApJL, 253, L61
Whitehurst R., King A., 1991, MNRAS, 249, 25